Improved Flux Pinning Performance of GdBCO Superconductor Bulks by Gd_3ZrO_7 Additions

J.Y. Zhang[a], Y.F. Zhang[a,*], Z.W. Lou[a], P.H. Zhang[a], C.Y. Li[a], J.W. Yuan[a], X.J. Zhang[a], L. Peng[a], Y.X. Ma[a], J.M. Xu[b], G.T. Yang[b] and M. Izumi[c]

[a] *College of Mathematics and Physics, Shanghai University of Electric Power, 1851 Hucheng Ring Road, New Pudong District, Shanghai 201306, People's Republic of China*
[b] *State Key Laboratory of Space Power Technology, Shanghai Institute of Space Power-Sources, Shanghai 200245, China*
[c] *Laboratory of Applied Physics, Tokyo University of Marine Science and Technology, 2-1-6 Etchujima, Koto-ku, Tokyo 135-8533, Japan*

Received: 22.01.2021 & Accepted: 06.06.2021

Doi: 10.12693/APhysPolA.140.40 *e-mail: 2009000018@shiep.edu.cn

Four $GdBa_2Cu_3O_{7-\delta}$ (GdBCO or Gd_{123}) superconductor bulks doped with different amounts of Gd_3ZrO_7 particles have been successfully prepared by the modified top-seeded melt-texture growth. Superconducting properties and microstructures of these bulks have been investigated in detail. All GdBCO bulks exhibit superior superconductivity with the onset critical temperature ($T_{c,onset}$) above 94 K, and the highest critical current density (J_c) of 49.1 kA/cm^2 was obtained in the GdBCO bulk doped with 0.8 mol.% Gd_3ZrO_7 particles at 77 K in self-field. During the top-seeded melt-texture growth process, the Gd_3ZrO_7 additions can react with the GdBCO phase, forming the $BaZrO_3$ particles and intensifying the Gd/Ba substitution, which can improve the flux pinning performance of the GdBCO bulk. As a result, J_c was enhanced and the trapped flux density significantly increased with the increase of Gd_3ZrO_7 additions. The maximum trapped flux density of 0.56 T obtained in the GdBCO bulk with 0.8 mol.% Gd_3ZrO_7 additions is more than three times as high as that of the undoped bulk. The squared stripes around the seed crystal were found in the doped bulks, and were identified as the macroscopic appearance of inhomogeneous microstructure in which the Gd_2BaCuO_5 (Gd211) free region and the Gd211-containing region were separated by a $BaZrO_3$-and-Ag layer in a small region. But such microstructural inhomogeneity can be well improved with the increase of Gd_3ZrO_7 additions. All these results show that Gd_3ZrO_7 additions improve the pinning performance of GdBCO superconductor bulks.

topics: GdBCO superconductor bulk, top-seeded melt-texture growth, Gd_3ZrO_7 additions, critical current density

1. Introduction

Because of higher critical current density (J_c) and the ability to trap higher magnetic field compared with the low temperature superconductors, $REBa_2Cu_3O_{7-\delta}$ (REBCO or RE123, RE = rare earth elements, such as Y, Gd, Sm, Nd, etc.) high temperature superconductors have attracted widespread attention and been widely used in various practical applications, such as magnetic levitation, motors, flywheel energy storage systems, etc. [1–5]. However, the improvement of superconducting property is greatly restricted due to the existence of weak links between the superconducting grains, the poor magnetic flux pinning ability, etc. The top-seeded melt-texture growth (TSMG) method has been widely used to prepare REBCO superconductor bulks with excellent properties, but the shrinkage of REBCO bulks due to the diffusion and loss of liquid phase during crystal growth can degrade the superconductivity of REBCO bulks and even lead to the failure of sample preparation. Meanwhile, the top-seeded infiltration and growth (TSIG) allows to avoid such problems and to have a negligible shrinkage of the bulks since the introduction of a liquid phase source can provide the sufficient liquid phase to the precursor pellet [6–9]. Consequently, in this study, we prepare the GdBCO superconductor bulks by the TSMG method and introduce the Y123 pellet as the liquid phase source in order to prepare high-performance GdBCO superconductor bulks with negligible shrinkage.

It has been proved that J_c and trapped magnetic flux of the REBCO superconductor bulk can be improved by introducing appropriate second phase particles as effective pinning centers [10–12] while Zr-containing particles can be used as effective doping particles to promote the improvement of REBCO superconductors [13–15] performance. In addition, considering that the second peak effect caused by the Gd/Ba substitution can well improve the J_c property in intermediate and high fields, we chose the Gd_3ZrO_7 particles as the doping particles. Generally, the optimal amount of the doping particles is around 0.4 mol.% [14, 16–19], thus the doping amount of the Gd_3ZrO_7 particles was set in the range of 0.0–0.8 mol.% in this study.

Four GdBCO superconductor bulks doped with 0.0–0.8 mol.% Gd_3ZrO_7 particles have been successfully fabricated by the modified TSMG method. We systematically studied the influence of different doping amounts of Gd_3ZrO_7 particles on the critical temperature, the critical current density, the trapped flux density and the microstructure of these GdBCO superconductor bulks.

2. Experimental

2.1. Preparation of Gd_3ZrO_7 powders

The Gd_3ZrO_7 powders have been prepared by solid state reaction. Commercial Gd_2O_3 (99.9%) and ZrO_2 (99.9%) powders were mixed in the molar ratio of Gd:Zr=3:1 and ground in a mortar for 3 h. We put the well mixed powders into the resistance furnace for sintering, with sintering temperature up to 940° in 5 h, and keeping for 10 h. Then, we ground the sintered powders again for 3 h and sintered again as before. After three times of sintering and four times of grinding, the Gd_3ZrO_7 powders were prepared. The XRD analysis was applied to identify the composition of powders, and the XRD diffraction patterns of powders are given in Fig. 1. It was found that the main peak of the XRD diffraction patterns is obvious, which confirms the successful preparation of the Gd_3ZrO_7 powders with high purity.

2.2. Preparation of GdBCO superconductor bulks

The Gd_3ZrO_7 powders and commercially pure powders of Gd123 (99.9%) and Gd_2BaCuO_5 (Gd211) (99.9%) were used as a starting material in an initial composition of Gd123 +40 mol.% Gd211+x mol.% Gd_3ZrO_7 ($x = 0$, 0.2, 0.4, 0.8), which are denoted as S0, S2, S4 and S8, respectively. In order to improve the mechanical property and inhibit the coarsening of Gd211 particles, 10 wt% Ag_2O and 0.5 wt% Pt were also added. The precursor powders were mixed thoroughly in a ball milling machine and then pressed into a cylinder pellet with the diameter of 25 mm and the thickness of 12 mm as the precursor pellet. Commercially pure Y123 powders were also pressed into a cylinder pellet with the diameter of 25 mm and the thickness of 3 mm as the liquid phase source pellet. The Y123 pellet was put under the GdBCO precursor to provide sufficient liquid phase to the precursor pellet. A NdBCO seed crystal, whose size is $2\times2\times0.5$ mm^3, was placed at the center of the top surface of the precursor pellet. The Y_2O_3 pellet was put under the Y123 pellet to avoid the reaction between Al_2O_3 substrate and liquid phase source. The entire arrangement was put into a box furnace for the TSMG process. The temperature profile is as follows. The maximum temperature (T_{max}) was set at 1079° and kept for 1 h, then it was reduced to 1008°, followed by cooling at a rate of 0.3°/h for 30° and finally cooled to room temperature. Subsequently, the annealing process was carried out in the high purity oxygen flow to transform the structure from the tetragonal non-superconducting phase to the orthogonal superconducting phase. The sintered samples were firstly heated to 450° in 5 h and kept for 40 h, followed by slowly cooling to 350° in 140 h, and then the temperature was decreased to 300° in 30 h. Finally, it was cooled down to room temperature. The details of the preparation process are described in [13, 19].

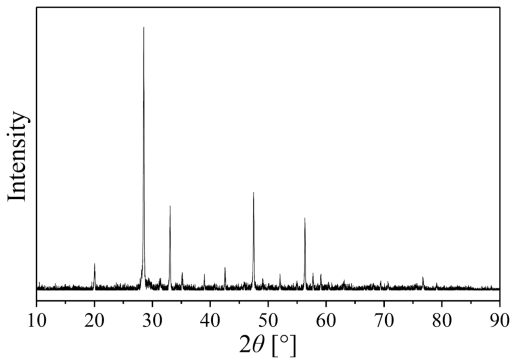

Fig. 1. XRD diffraction patterns of Gd_3ZrO_7 powders prepared by solid state reaction.

2.3. Measurement of characteristics

For the measurement of trapped flux density, the bulks were cooled down to the liquid nitrogen temperature under a magnetic field of 1 T. After 30 minutes, the applied field was removed and the distribution of the trapped flux density could be obtained by the Hall probe sensor with the distance of 0.5 mm between the probe and the sample surface. In order to study the effect of Gd_3ZrO_7 additions on the superconducting property of the GdBCO superconductor bulk, small rectangular specimens with the size of $2 \times 2 \times 1$ mm^3 were cut from different positions of these superconductor bulks for the measurement of their superconducting properties. Two specimens were cut under the seed, labeled as C1 and C2 based on the distance from the top surface to the bottom, and two other specimens were cut

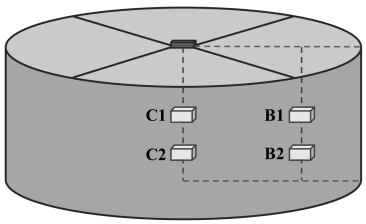

Fig. 2. Schematic diagram of the positions of four specimens cut from the GdBCO superconductor bulk.

near the boundary, labeled as B1 and B2 based on the distance from the top surface to the bottom. The specific positions of these specimens have been given in Fig. 2.

The DC magnetization measurements were carried out by using the physical property measurement system (PPMS), and the J_c values were deduced based on the extended Bean critical state model [20]. The microstructures of these bulks were observed through the scanning electron microscope (SEM), while the elemental distribution was analyzed by the energy-dispersive X-ray spectroscopy (EDX).

3. Results and discussion

Four single domain GdBCO superconductor bulks with different doping amounts of Gd_3ZrO_7 particles have been successfully fabricated by the modified TSMG method, as shown in Fig. 3. It can be seen that the NdBCO seed crystals of all bulks are kept intact and the fourfold growth sector can be clearly observed, which means good single domain performances of these four GdBCO superconductor bulks. An interesting phenomenon is observed in which the bulks doped with the Gd_3ZrO_7 particles show squared stripes around the seed crystal, in contrast to undoped bulk where this phenomenon does not occur. So we infer that the squared stripes are caused by the Gd_3ZrO_7 particles. In some studies on the REBCO superconductor bulks doped with ZrO_2 powders [18–21], inhomogeneous microstructures were proposed, such as the second phase free band–the second phase rich band–the second phase diluted band and a growth cycle consisting of a RE211 free layer–porous narrow layer–RE211 high concentration layer. In [22], the structure that the squared narrow bands formed by $BaZrO_3$ and Y211 particles enclosing the YBCO single domain regions free of Y211 particles was considered in the YBCO bulk with $BaZrO_3$ additions. According to these studies, it is reasonable to deduce that the squared stripes around the seed crystal shown in the doped samples are the macroscopic appearances of inhomogeneous microstructure. Moreover, it can be found that the region where the squared stripes are distributed becomes smaller with the increase of Gd_3ZrO_7 additions.

Fig. 3. Top view of GdBCO superconductor bulks with different doping amounts of Gd_3ZrO_7 particles: (a) S0, (b) S2, (c) S4, (d) S8.

The temperature dependence of magnetization of specimens cut from different positions, C1, C2, B1 and B2, of the GdBCO superconductor bulks with different amounts of Gd_3ZrO_7 particles are shown in Fig. 4. The case of the position dependence of $T_{c,\,\mathrm{onset}}$ of specimens cut from four GdBCO superconductor bulks with different amount of Gd_3ZrO_7 particles was presented in Fig. 4e. It can be clearly seen that except for B1 position, the $T_{c,\,\mathrm{onset}}$ values of some doped bulks are slightly lower than that of the undoped bulk. However, the addition of Gd_3ZrO_7 particles does not degrade the superconductivity of GdBCO bulk because all specimens exhibit high $T_{c,\,\mathrm{onset}}$ values ranging from 94.2 K to 95.9 K.

Figure 5 shows the magnetic field μH dependence of critical current density J_c of specimens, cut from different positions (C1, C2, B1 and B2) of the GdBCO superconductor bulks with different amounts of Gd_3ZrO_7 particles at 77 K. Plots of J_c in self-field as a function of the amount of Gd_3ZrO_7 additions are shown in Fig. 6, in order to present the occurrence of these bulks in low fields. The J_c values of specimens cut from different positions of a superconductor bulk are usually different, and there are various causes of that, e.g., the existence of a seed crystal, the inhomogeneous distribution of the second phase particles, etc. [6, 23, 24]. Based on the results shown in Figs. 5 and 6, we can also find that there are larger or smaller differences between the four specimens for both undoped and doped bulks, however these differences decrease in the doped bulks as compared with the undoped bulk. This indicates that the addition of the Gd_3ZrO_7 particles has a position effect on the microstructural uniformity.

It can be seen in Fig. 6 that the self-field J_c of the specimens under the seed (C1 and C2) increases, however such increase is not obvious in the GdBCO bulk doped with 0.8 mol.% Gd_3ZrO_7 particles, where a significant decrease of J_c is observed at C1 position. For the specimens near the boundary (B1 and B2), the self-field J_c is degraded by the

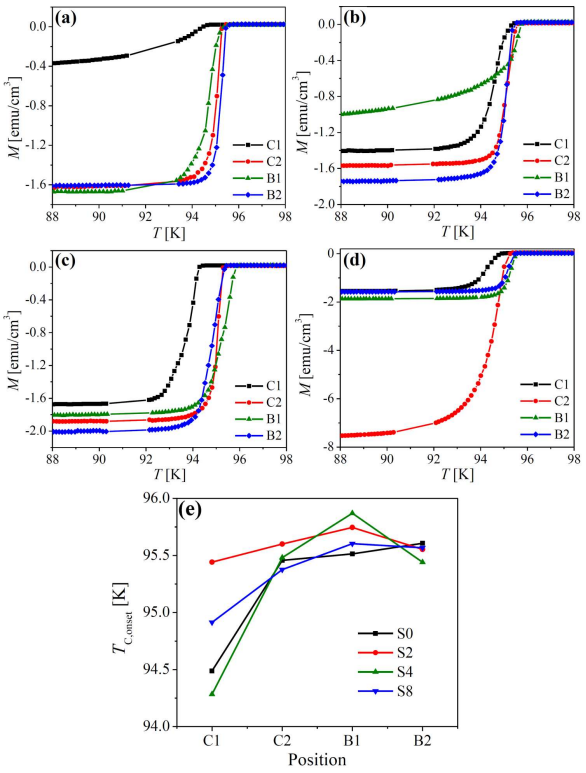

Fig. 4. Temperature (T) dependence of magnetization (M) of specimens cut from different positions, C1 (squares), C2 (circles), B1 (triangles), and B2 (diamonds), of the GdBCO superconductor bulks with different amounts of Gd_3ZrO_7 particles: (a) S0, (b) S2, (c) S4, (d) S8. (e) Position dependence of $T_{c,onset}$ of specimens cut from four GdBCO superconductor bulks with different amounts of Gd_3ZrO_7 particles: S0, S2, S4, and S8.

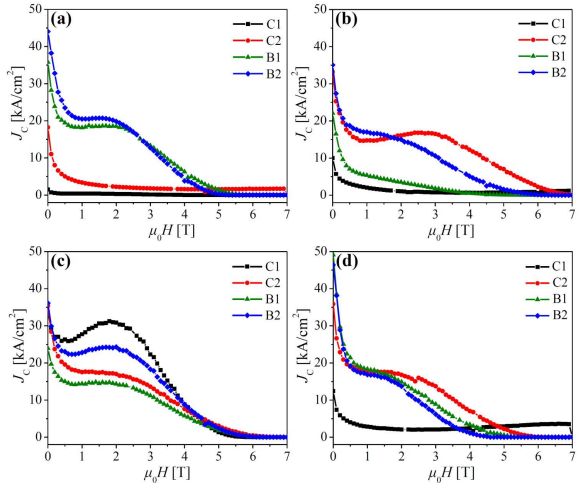

Fig. 5. Magnetic field (μH) dependence of critical current density (J_c) of specimens cut from different positions, C1 (squares), C2 (circles), B1 (triangles) and B2 (diamonds) of the GdBCO superconductor bulks with different amount of Gd_3ZrO_7 particles: (a) S0, (b) S2, (c) S4, (d) S8 at 77 K.

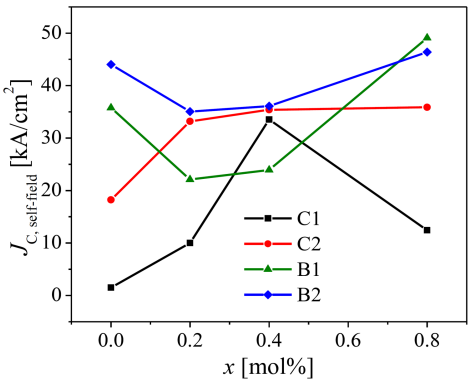

Fig. 6. Plots of J_c in self-field ($J_{c,self-field}$) of specimens from different positions, C1 (squares), C2 (circles), B1 (triangles) and B2 (diamonds) as a function of the amount of Gd_3ZrO_7 additions (x).

Gd_3ZrO_7 additions first, and then improved with the increase of the Gd_3ZrO_7 additions. The maximum self-field $J_c = 49.1$ kA/cm^2 at 77 K is obtained in the B1 of the GdBCO bulk doped with 0.8 mol.% Gd_3ZrO_7 particles. In addition, it can be observed that the second peak effect becomes more obvious with the addition of Gd_3ZrO_7 particles, but less obvious in the GdBCO bulk doped with 0.8 mol.% Gd_3ZrO_7 particles.

For the undoped bulk (S0), the J_c values of specimens near the boundary are higher than those of specimens under the seed (B1>C1 and B2>C2) in low fields. It is a typical phenomenon of REBCO superconductor bulks [25]. During the growth of REBCO single domain superconductor bulks, small-sized Gd211 particles are pushed to the growth front due to the pushing/trapping theory [21, 25, 26] and serve as pinning centers greatly improving their J_c properties. This, in turn, results in higher J_c of specimens near the boundary than that of the specimens under the seed in low fields. The slight second peaks are shown in B1 and B2 of the undoped bulk, which are usually caused by the Gd/Ba substitution.

One can observe in Figs. 5 and 6 that when a small amount of Gd_3ZrO_7 particles was introduced into the GdBCO superconductor bulks (S2), the self-field J_c values of the specimens under the seed increased, while the self-field J_c values of the specimens near the boundary decreased. It can be inferred that the small doping amount of the Gd_3ZrO_7 particles cannot well improve the J_c property of the whole GdBCO bulk in low fields. In intermediate and high fields, however, the J_c properties were well improved, especially for C2 of S2, exhibiting a clear second peak in the $J_c(H)$ dependence. In the case of the GdBCO bulk doped with 0.4 mol.% Gd_3ZrO_7 particles (S4), the J_c property in low fields was slightly improved, while a significant improvement of J_c for almost all specimens was observed in intermediate and high fields where a clear second peak appears. Although S8 do not

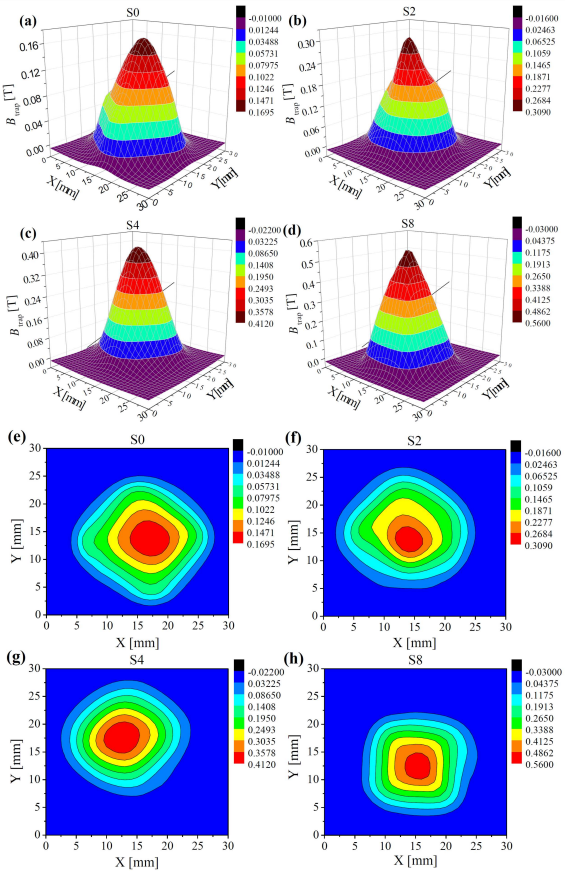

Fig. 7. Trapped flux density (B_{trap}) of GdBCO superconductor bulks with different doping amounts of Gd_3ZrO_7 particles: (a) S0, (b) S2, (c) S4, (d) S8; parts (e), (f), (g), and (h) are the top view of (a), (b), (c), and (d), respectively.

exhibit the secondary peak, the self-field J_c of S8 was significantly improved, especially for the specimens near the boundary. Therefore, we infer that the addition of Gd_3ZrO_7 particles has a relevant impact on the improvement of J_c property in the whole field range, and the Gd_3ZrO_7 additions may intensify the Gd/Ba substitution.

Figure 7 shows the trapped flux density (B_{trap}) of GdBCO superconductor bulks with different doping amounts of Gd_3ZrO_7 particles. It is clear that the trapped field profiles of all samples exhibit good symmetry and conical shape, meaning that both undoped and doped GdBCO bulks exhibit superior single domain properties [1, 14, 27, 30]. It can be found, in addition, that the trapped field of GdBCO bulks continuously increase with the doping amount of Gd_3ZrO_7 particles. The maximum trapped flux density value of 0.56 T is obtained in the bulk doped with 0.8 mol.% Gd_3ZrO_7 particles. Note that it is more than three times as high as that of the undoped bulk whose maximum trapped flux density value is 0.17 T. The trapped flux density B_{trap} is proportional to the grain size and J_c, according to the equation $B_{\mathrm{trap}} = A\mu J_c R$, where A is the constant, μ is the permeability of vacuum, J_c is the

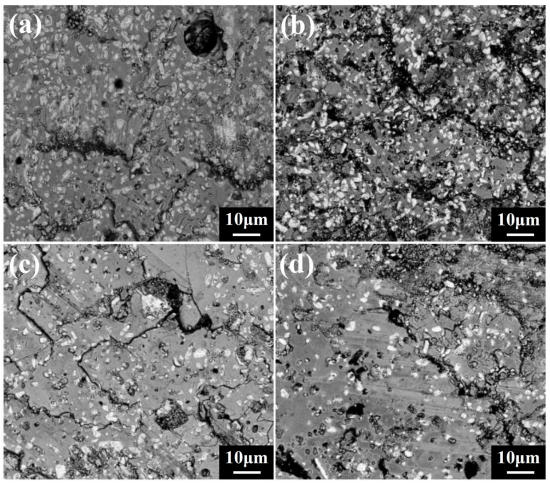

Fig. 8. SEM micrographs (at a magnification of 3000×) of B1 specimens of the GdBCO superconductor bulks with different doping amounts of Gd_3ZrO_7 particles: (a) S0, (b) S2, (c) S4, (d) S8.

critical current density and R is the radius of the grain [1, 31, 32]. Since there is little difference in sizes between these bulks, we can conclude that the enhancement of B_{trap} is mainly due to the increase of J_c with the increase of the Gd_3ZrO_7 additions. Therefore, it further proves that Gd_3ZrO_7 additions play a crucial role in improving the J_c property, thus enhancing the trapped flux density of the GdBCO superconductor bulk.

A high-performance superconductor must have an ideal microstructure, and the size and distribution of the second phase particles are important for its superior superconductivity. In general, the Gd211 particles with the appropriate size can be used as the pinning centers, increasing the J_c values of the superconductor bulks [26, 28, 33]. The SEM micrographs of B1 specimens of the GdBCO superconductor bulks with different doping amount of Gd_3ZrO_7 particles are presented in Fig. 8, from which the distribution of the Gd211 particles can be observed. The white particles, which are identified as the Gd211 particles, are distributed in the four samples. Obviously, the content of the Gd211 particles distributed in the B1 specimen of the GdBCO bulk continuously decreases with the increase of Gd_3ZrO_7 additions. The causes of this phenomenon will be systematically analyzed later.

In order to further analyze the Gd211 particles distributed in these GdBCO bulks, the size of the Gd211 particles shown in Fig. 8 was counted by the software of Nano measurer 1.2, as shown in Fig. 9. The horizontal axis shows the size range, while the vertical axis shows the number of the Gd211 particles within a certain size range as a percentage of the total number of the Gd211 particles counted in each sample. The curves are obtained by fitting the size distribution of the Gd211 particles and are represented by the red solid curves in Fig. 9, thus the size distribution and the average size of the Gd211

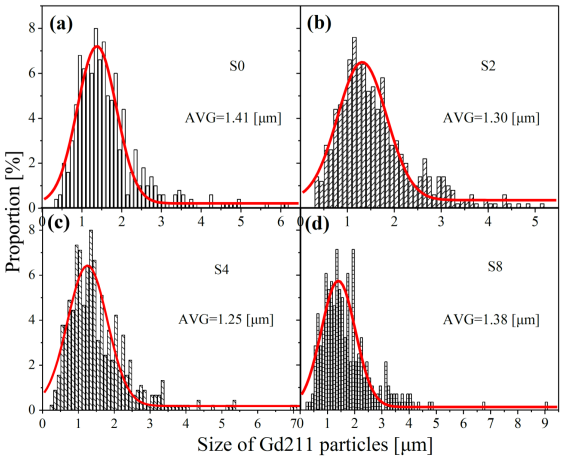

Fig. 9. The size distribution of the Gd211 particles in the GdBCO superconductor bulks with different doping amounts of Gd_3ZrO_7 particles: (a) S0, (b) S2, (c) S4, (d) S8. The red solid curves represent the fitted curves obtained by fitting the size distribution of the Gd211 particles. The average size values of the Gd211 particles (AVG) obtained from the peak position of each fitted curve are also given.

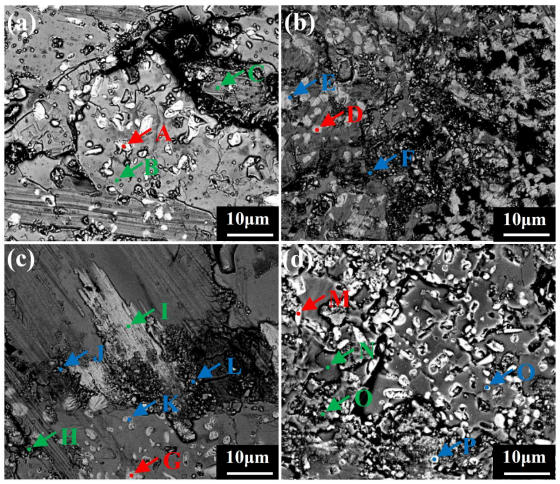

Fig. 10. SEM micrographs (at a magnification of 5000×) of specimens at B1 position of the GdBCO superconductor bulks with different doping amounts of Gd_3ZrO_7 particles: (a) S0, (b) S2, (c) S4, (d) S8. The Gd211 particles, Gd123 phase and spot containing Gd211 particles, $BaZrO_3$ particles and liquid phase compound ($BaCuO_2$ + CuO) are marked with red dots, green dots, and blue dots, respectively.

particles in each bulk can be predicted. The average size values of the Gd211 particles (AVG) are obtained from the peak position of each fitted curve. The average size of the Gd211 particles decreases with the increase of Gd_3ZrO_7 additions when the doping amount is less than 0.8 mol.%, while the average size of the Gd211 particles in S8 increase compared with that in other doped bulks (S2 and S4). However, when compared with the undoped bulk, the average size of the Gd211 particles in all doped bulks decreases. We can infer, therefore, that the Gd_3ZrO_7 additions have a significant impact on the refinement of the Gd211 particles, but the excessive Gd_3ZrO_7 additions can make the Gd211 particles coarser as compared with the GdBCO bulk with a low doping amount.

Figure 10 exhibits the SEM diagrams at a higher magnification (5000×) of specimens at B1 position of the GdBCO superconductor bulks with different doping amounts of Gd_3ZrO_7 particles. The stoichiometry of various spots labeled in Fig. 10 were identified by EDS analysis and the results are listed in Table I. It can be seen that all doped bulks contain not only Gd211 particles, but also $BaZrO_3$ particles and liquid phase compound ($BaCuO_2$+CuO), as marked in Fig. 10 (spots E and F of S2, spots J, K and L of S4, as well as spots P and Q of S8). In many studies on REBCO superconductors doped with Zr-containing particles, the Zr-containing particles tend to react with RE123 and form $BaZrO_3$ particles [33–35]. Therefore, we infer that the reaction between Gd_3ZrO_7 particles and Gd123 phase also occurs in these doped bulks and produces $BaZrO_3$ particles, accompanied by a certain amount of liquid phase compound. In addition, it can be found that the molar ratio of Gd to Ba in the Gd123 phase of the doped bulks (spots H and I in S4 and spots N and O in S8) is higher than that of the undoped bulk (spots B and C in S0), that is, a more superconducting phase of doped bulks exists as the $Gd_{1+x}Ba_{2-x}Cu_3O_7$ phase. Considering the obvious second peak appeared in S2 and S4, we infer that the Gd_3ZrO_7 additions can intensify the Gd/Ba substitution in the GdBCO bulks. One can suggest that the following reactions may occur during the growth of GdBCO superconductor bulks:

$$GdBa_2Cu_3O_7 + Gd_3ZrO_7 \rightarrow BaZrO_3 + 4Gd^{3+} + BaCuO_2 + 2CuO, \quad (1)$$

$$Gd^{3+} + GdBa_2Cu_3O_7 \rightarrow Gd_{1+x}Ba_{2-x}Cu_3O_7, \quad (2)$$

$$2GdBa_2Cu_3O_7 \rightleftharpoons Gd_2BaCuO + 3BaCuO_2 + 2CuO. \quad (3)$$

Throughout the TSMG process, some part of the Gd123 phase reacts with Gd_3ZrO_7 particles generating $BaZrO_3$ particles and releasing Gd^{3+} ions, as shown with (1). At high temperature, some other part of the Gd123 phase decomposes and generates Gd211 particles, as shown with (3).

As shown in (2), the released Gd^{3+} ions can substitute for the Ba^{2+} ions in the crystal lattice of $GdBa_2Cu_3O_7$ and form the $Gd_{1+x}Ba_{2-x}Cu_3O_7$ phase. The $BaZrO_3$ particles were widely used as the doping particles in many studies and proved to have a significant effect on the improvement of the superconducting property of the REBCO superconductors [15, 34–38]. In addition, some studies proposed that the $BaZrO_3$ particles, which formed in the ZrO_2-doped Gd123 bulk can disperse in the bulk

TABLE I

Stoichiometry and possible particles of spots labeled in Fig. 10 identified by EDS analysis.

Sample	Spot	Gd [%]	Ba [%]	Cu [%]	Zr [%]	Possible particles
S0	A	19.2	10.5	10.9	0.0	Gd211
	B	7.9	16.1	24.5	0.0	Gd123 (Gd:Ba:Cu = 1:2.04:3.10)
	C	7.0	14.6	21.8	0.0	Gd123 (Gd:Ba:Cu = 1:2.09:3.11)
S2	D	21.9	12.0	12.6	0.0	Gd211
	E	10.9	15.0	11.7	7.0	109Gd211 + 140$BaZrO_3$ + 51$BaCuO_2$ + 74CuO
	F	1.5	15.3	5.1	9.8	15Gd211 + 196$BaZrO_3$ + 95$BaCuO_2$
S4	G	18.4	9.9	10.3	0.1	Gd211
	H	7.7	15.1	22.4	0.0	Gd123 (Gd:Ba:Cu = 1:1.96:2.91)
	I	3.8	7.2	11.8	0.0	Gd123 (Gd:Ba:Cu = 1:1.89:3.11)
	J	5.3	15.7	16.2	4.5	53Gd211 + 90$BaZrO_3$ + 171$BaCuO_2$ + 100CuO
	K	15.0	10.7	13.0	0.4	75Gd211 + 4$BaZrO_3$ + 28$BaCuO_2$ + 27CuO
	L	8.4	9.2	8.5	1.1	42Gd211 + 11$BaZrO_3$ + 39$BaCuO_2$ + 4CuO
S8	M	19.0	10.4	10.6	0.0	Gd211
	N	8.8	17.2	25.4	0.0	Gd123 (Gd:Ba:Cu = 1:1.95:2.89)
	O	8.2	15.1	22.7	0.0	Gd123 (Gd:Ba:Cu = 1:1.84:2.77)
	P	10.5	15.4	12.0	7.8	105Gd211 + 156$BaZrO_3$ + 47$BaCuO_2$ + 88CuO
	Q	9.7	15.3	14.7	5.7	97Gd211 + 114$BaZrO_3$ + 95$BaCuO_2$ + 102CuO

with the size of around 50 nm [34, 35] — the size small enough to treat the $BaZrO_3$ particles as the effective pinning centers. Therefore, as compared with the undoped bulk in which only Gd211 particles serve as the pinning centers, both $BaZrO_3$ particles and Gd211 particles — as the pinning centers in the doped bulks — can well improve the flux pinning performance of GdBCO superconductor bulks.

When the GdBCO bulk is doped with the Gd_3ZrO_7 particles, some part of the Gd123 phase reacts with Gd_3ZrO_7 particles and, since such a Gd123 phase decomposition occurs, only a few of the Gd211 particles remain. Moreover, the liquid phase compound produced by the reaction between Gd_3ZrO_7 particles and the Gd123 phase can continually react with the Gd211 particles to promote the growth of the Gd123 superconducting phase, which can also decrease the content of the Gd211 particles. During the TSMG process, the Gd211 particles generally accumulate under the seed and are pushed to the growth front according to the pushing/trapping theory [21, 25, 26]. However, the decrease of the content of Gd211 particles can weaken the pushing effect, leading to fewer Gd211 particles to be pushed to the boundary.

This can well explain the phenomenon that the content of the Gd211 particles at the B1 position decreases with the increase of Gd_3ZrO_7 additions, as shown in Fig. 8. The $BaZrO_3$ particles formed by the reaction between Gd_3ZrO_7 particles and Gd123 phase tend to accumulate at the early stage of crystal growth, that is, at the region under the seed. They diffuse to the boundary during the crystal growth. When the doping amount of the Gd_3ZrO_7 particles is low, the content of the $BaZrO_3$ particles is low, thus the $BaZrO_3$ particles are mainly distributed under the seed. As a result, the content of the $BaZrO_3$ particles under the seed is higher than that near the boundary. When the doping amount of the Gd_3ZrO_7 particles is higher, the content of the $BaZrO_3$ particles under the seed increases, and continuously diffuses to the boundary during the TSMG process.

Hence, we impose a view that for the low doping amount of the Gd_3ZrO_7 particles, the increase of the self-field J_c at the position under the seed is due to the fact that more $BaZrO_3$ particles accumulate under the seed and thus serve as the pinning centers (although the content of Gd211 particles under the seed decreases). However, for the high doping amount of the Gd_3ZrO_7 particles, less accumulation of the $BaZrO_3$ particles greatly degrades the self-field J_c property under the seed. It is due to the Gd_3ZrO_7 diffusion and the significant decrease of the content of Gd211 particles under the seed. It may be the reason why the self-field J_c of the specimens under the seed increases first, but insubstantially and even decreases significantly at the C1 position when the Gd_3ZrO_7 additions reach 0.8 mol.%, as shown in Fig. 6. While in the region near the boundary, when the doping amount of the Gd_3ZrO_7 particles is low, the $BaZrO_3$ particles mainly accumulate under the seed, thus there are few $BaZrO_3$ particles as pinning centers near the boundary.

Additionally, the decrease of the content of Gd211 particles pushed to the boundary can also degrade the J_c properties of the specimens near the boundary. Therefore, the self-field J_c of the specimens near the boundary in S2 decreases, as compared with the undoped bulk. As the Gd_3ZrO_7 additions increase, more $BaZrO_3$ particles are formed and serve as the flux pinning centers. Further, such $BaZrO_3$ particles can diffuse to the boundary during

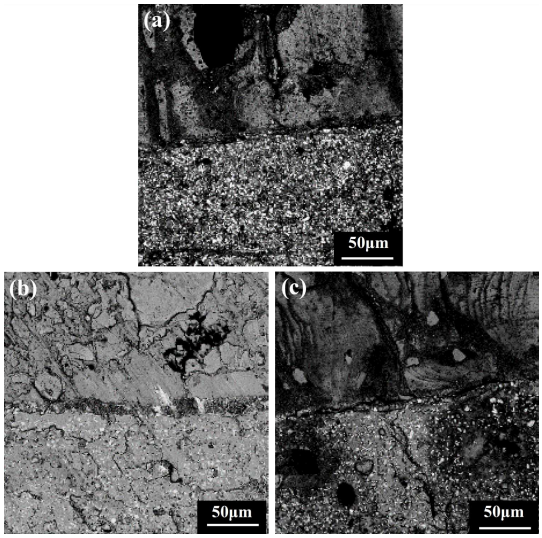

Fig. 11. SEM micrographs (at a magnification of 1000×) of the peculiar microstructure in doped GdBCO superconductor bulks with different amounts of Gd_3ZrO_7 particles: (a) S2, (b) S4, (c) S8.

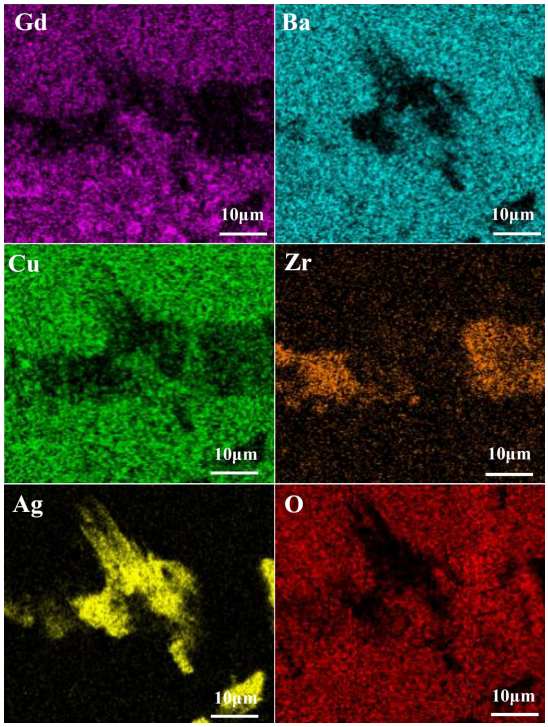

Fig. 12. EDS elemental maps of B1 specimen in S4 corresponding to Fig. 10c.

the crystal growth, which results in higher self-field J_c values of the specimens near the boundary with the addition of the Gd_3ZrO_7 particles. It is the reason why the self-field J_c of the specimens near the boundary decreases first, then increases with the increase of Gd_3ZrO_7 additions, as shown in Fig. 6. Since the amount of the $BaZrO_3$ particles is high in B1 of S8, the critical radius of the Gd211 particle increases [22], that is, some Gd211 particles with a slightly larger size trapped in the GdBCO bulk doped with a smaller amount of the Gd_3ZrO_7 additions can be pushed to the boundary in S8, thus enhancing the average size of the Gd211 particles in B1 of S8. It may be the reason why the average size of Gd211 particles in S8 is higher than that of Gd211 particles in S2 and S4, as shown in Fig. 9.

In general, the J_c of REBCO bulks in low fields depends more on the δl pinning, while the J_c of REBCO bulks in intermediate and high fields depends more on the δT_c pinning. In this study, the addition of Gd_3ZrO_7 particles provides more $BaZrO_3$ particles as the pinning centers and intensifies the Gd/Ba substitution. The former can lead to the δl pinning centers which increase J_c in low fields, while the latter can result in the δT_c pinning centers which can increase J_c in intermediate and high fields and can be reflected by the second peak effect [5, 39]. In fact, they cause the improvement of the J_c property by doping Gd_3ZrO_7 particles, and the continuous increase of the trapped flux density with the increase of Gd_3ZrO_7 additions.

It can also be observed in Fig. 10 that the microstructure of the B1 of S4 exhibits obvious inhomogeneity. However, this peculiar microstructure is not unique to S4. Also, we can find such microstructural inhomogeneity in S2 and S8, as shown in Fig. 11 which gives SEM micrographs of doped GdBCO bulks at a lower magnification of 1000×. Figure 11b is a SEM diagram of the B1 specimen in S4 shown in Fig. 10c at a lower magnification. Figure 12 shows EDS elemental maps of the B1 specimen in S4 corresponding to Fig. 10c. It can be found that all doped samples form the microstructure with the Gd211-free region and the Gd211-containing region separated by a special layer. The composition of this special layer was analyzed by EDS analysis (see Fig. 12). By combining EDS elemental maps in Fig. 12 and stoichiometry of spots J and L in this special layer shown in Fig. 10 and Table I, we can draw the following conclusion: the special layer, which separates the Gd211 free region and the Gd211-containing region is mainly made of $BaZrO_3$ particles and Ag particles. Some studies on the REBCO bulks doped with Zr-containing particles have already proposed the idea of inhomogeneous microstructure [18, 21] and the phenomenon that Zr-containing particles tend to accumulate around silver [14]. Therefore, we also infer that during the TSMG process, $BaZrO_3$ particles formed by a reaction between Gd_3ZrO_7 particles and the Gd123 phase can accumulate along with Ag and form the layer. This, in fact, can result in the formation of an inhomogeneous microstructure in which the Gd211 free region and the Gd211-containing region were separated by the $BaZrO_3$–and–Ag layer in a small region. Such an inhomogeneous microstructure results in the appearance of squared stripes around the seed crystal in the doped GdBCO superconductor bulks. According to Fig. 3,

the region where the squared stripes are distributed becomes smaller with the increase of Gd_3ZrO_7 additions. It means that the microstructural uniformity can be improved with increasing Gd_3ZrO_7 additions, which is consistent with the previous analysis.

Some studies on the REBCO bulks doped with Zr-containing particles have already proposed the idea of inhomogeneous microstructure [18, 21] and the phenomenon that Zr-containing particles tend to accumulate around silver [14].

4. Conclusion

In this study, we have successfully prepared four $GdBa_2Cu_3O_{7-\delta}$ (GdBCO) single domain superconductor bulks doped with 0–0.8 mol.% Gd_3ZrO_7 particles by the modified TSMG method. The Gd_3ZrO_7 powders were prepared by solid state reaction and the single phase and high purity were identified by XRD analysis. The superconducting properties, such as critical temperature (T_c), critical current density (J_c) and trapped flux density (B_{trap}), as well as the microstructure of these GdBCO bulks have been systematically analyzed. The onset critical temperature ($T_{c,onset}$) of all GdBCO superconductor bulks are above 94 K, meaning the successful preparation and superior superconductivity.

The reaction between Gd_3ZrO_7 particles and Gd123 phase occurs during the TSMG process, forming the $BaZrO_3$ particles and intensifying the Gd/Ba substitution which leads to the δl pinning centers and δT_c pinning centers, respectively. Such an improvement of flux pinning performance significantly enhances J_c and the trapped flux density. The highest self-field J_c of 49.1 kA/cm^2 was obtained in the GdBCO bulk doped with 0.8 mol.% Gd_3ZrO_7 particles. Along with doping, the self-field J_c of the specimens under the seed first increases and then, in the case of the C1 position, it significantly decreases when the doping amount of Gd_3ZrO_7 particles reaches 0.8 mol.% while the self-field J_c of the specimens near the boundary decreases first, and then increases with the increase of the Gd_3ZrO_7 additions. It is due to the combined effect of the Gd_2BaCuO_5 (Gd211) particles and the $BaZrO_3$ particles according to the SEM and EDS analysis. The trapped flux density of GdBCO bulks continuously increases with the doping amount of Gd_3ZrO_7 particles, and the maximum trapped flux density of 0.56 T is obtained in the bulk doped with 0.8 mol.% Gd_3ZrO_7 particles, which is more than three times as high as that of the undoped bulk whose maximum flux density is 0.17 T.

The doped bulks exhibit squared stripes around the seed crystal, which are identified as the macroscopic appearance of the inhomogeneous microstructure in which the Gd_2BaCuO_5 (Gd211) free region and the Gd211-containing region were separated by the $BaZrO_3$–and–Ag layer in a small region. The region where squared stripes are distributed becomes smaller with the increase of Gd_3ZrO_7 particles, which means the microstructural inhomogeneity can be improved by the addition of the Gd_3ZrO_7 particles. These results confirm that the superconducting properties and microstructural uniformity of the GdBCO superconductor bulk can be well improved by doping Gd_3ZrO_7 particles, which is of significance for the industrial applications of superconductors.

Acknowledgments

This work was supported by the National Natural Science Foundation of China (grant No. 11004129), the Scientific Research Starting Foundation for the Returned Overseas Chinese Scholars, the Ministry of Education of China (SRF for ROCS, SEM), the Innovation Program of Shanghai Municipal Education Commission, China (grant No. 11YZ197, 12ZZ174), and the Shanghai Natural Science Foundation, China (grant No. 16ZR1422700).

References

[1] T. Ida, Z. Li, D.F. Zhou, M. Miki, Y.F. Zhang, M. Izumi, *Supercond. Sci. Technol.* **29**, 054005 (2016).

[2] J. Wang, S. Wang, Y. Zeng et al., *Physica C* **378-381**, 809 (2002).

[3] N. Koshizuka, *Physica C* **445-448**, 1103 (2006).

[4] P. Mukherjee, V.V. Rao, *Physica C* **563**, 67 (2019).

[5] Y.F. Zhang, D.F. Zhou, T. Ida, M. Miki, M. Izumi, *Supercond. Sci. Technol.* **29**, 044005 (2016).

[6] K. Zmorayova, L. Vojtkova, T. Hlasek, J. Plechacek, P. Diko, *Supercond. Sci. Technol.* **33**, 034005 (2020).

[7] W.M. Yang, X.D. Guo, F. Wan, G.Z. Li, *Cryst. Growth Des.* **11**, 3056 (2011).

[8] Z.L. Feng, W.M. Yang, J.W. Li, M. Wang, Y.X. Yang, Z.B. Gao, X.N. Huang, *J. Supercond. Nov. Magn.* **33**, 1559 (2020).

[9] L. Vojtkova, P. Diko, S. Piovarči, *Acta Phys. Pol. A* **131**, 1048 (2017).

[10] S.P.K. Naik, M. Muralidhar, M. Murakami, *J. Supercond. Nov. Magn.* **31**, 981 (2018).

[11] P. Hajdova, I. Shepa, E. Mudra, M. Rajnak, J. Dusza, P. Diko, *Acta Phys. Pol. A* **137**, 800 (2020).

[12] D. Volochová, P. Diko, S. Piovarči, V. Antal, J. Kováč, M. Jirsa, *Acta Phys. Pol. A* **131**, 1009 (2017).

[13] Y.F. Zhang, M. Izumi, Y.J. Li, M. Murakami, T. Gao, Y.S. Liu, P.L. Li, *Physica C* **471**, 840 (2011).

[14] D.F. Zhou, M. Izumi, T. Fujimoto, Y.F. Zhang, W.L. Zhou, K. Xu, *IEEE Trans. Appl. Supercond.* **25**, 6800204 (2015).

[15] F. Wang, H. Tian, *J. Mater. Sci. Mater. Electron.* **30**, 4137 (2019).

[16] C. Xu, A. Hu, N. Sakai, M. Izumi, I. Hirabayashi, *Supercond. Sci. Technol.* **18**, 1082 (2005).

[17] K. Xu, D.F. Zhou, B.Z. Li, S. Hara, Z.G. Deng, M. Izumi, *Physica C* **510**, 54 (2015).

[18] C. Xu, A. Hu, N. Sakai, M. Izumi, I. Hirabayashi, *Physica C* **445-448**, 357 (2006).

[19] Y. Zhang, M. Izumi, Y. Kimura, Y. Xu, *Physica C* **469**, 1169 (2009).

[20] D.X. Chen, R.B. Goldfarb, *J. Appl. Phys.* **66**, 2489 (1989).

[21] K. Iida, N.H. Babu, E.S. Reddy, Y.H. Shi, D.A. Cardwell, *Supercond. Sci. Technol.* **18**, 249 (2004).

[22] A.E. Carrillo, T. Puig, J. Plain, J. Figueras, X. Obradors, *Physica C* **336**, 213 (2000).

[23] V. Antal, K. Zmorayova, M. Rajnak, L. Vojtkova, T. Hlasek, J. Plechacek, P. Diko, *Supercond. Sci. Technol.* **33**, 044004 (2020).

[24] P. Hajdova, K. Zmorayova, M. Rajnak, P. Diko, *Supercond. Sci. Technol.* **33**, 034003 (2020).

[25] Y.H. Shi, D.K. Namburi, W. Zhao, J.H. Durrell, A.R. Dennis, D.A. Cardwell, *Supercond. Sci. Technol.* **29**, 015010 (2016).

[26] W. Zhai, Y.H. Shi, J.H. Durrell, A.R. Dennis, D.A. Cardwell, *Cryst. Growth Des.* **14**, 6367 (2014).

[27] D.A. Cardwell, Y.H. Shi, N.H. Babu, S.K. Pathak, A.R. Dennis, K. Iida, *Supercond. Sci. Technol.* **23**, 034008 (2010).

[28] S. Nariki, S.J. Seo, N. Sakai, M. Murakami, *Supercond. Sci. Technol.* **13**, 778 (2000).

[29] D. Zhou, S. Hara, B. Li, J. Noudem, M. Izumi, *Supercond. Sci. Technol.* **27**, 044015 (2014).

[30] D. Volochová, K. Jurek, M. Radušovská, S. Piovarči, V. Antal, J. Kováč, M. Jirsa, P. Diko, *Acta Phys. Pol. A* **126**, 358 (2014).

[31] C.P. Bean, *Rev. Mod. Phys.* **36**, 31 (1964).

[32] H.P. Liao, J. Zheng, L.W. Jin, H. Huang, Z.G. Deng, Y.H. Shi, D.F. Zhou, D.A. Cardwell, *Supercond. Sci. Technol.* **31**, 035010 (2018).

[33] W.M. Yang, X.C. Yuan, C.Y. Zhang, *IEEE Trans. Appl. Supercond.* **29**, 6802505 (2019).

[34] K.D. Keukeleere, P. Cayado, A. Meledin et al., *Adv. Electron. Mater.* **2**, 1600161 (2016).

[35] A. Hu, C. Xu, M. Izumi, I. Hirabayashi, M. Ichihara, *Appl. Phys. Lett.* **89**, 192508 (2006).

[36] C. Xu, A. Hu, M. Ichihara, M. Izumi, Y. Xu, N. Sakai, I. Hirabayashi, *Jpn. J. Appl. Phys.* **48**, 023002 (2009).

[37] S. Kang, A. Goyal, J. Li et al., *Science* **311**, 1911 (2006).

[38] A. Xu, Y. Zhang, M.H. Gharahcheshmeh et al., *Sci. Rep.* **7**, 6853 (2017).

[39] M.R. Koblischka, A.J.J. van Dalen, T. Higuchi, S.I. Yoo, M. Murakami, *Phys. Rev. B* **58**, 2863 (1998).